⌘ *Author's Choice*

THE JOURNAL OF BIOLOGICAL CHEMISTRY VOL. 286, NO. 8, pp. 6554–6565, February 25, 2011

Structure and Dynamics of the First Archaeal Parvulin Reveal a New Functionally Important Loop in Parvulin-type Prolyl Isomerases*[S]

Received for publication, July 2, 2010, and in revised form, November 17, 2010 Published, JBC Papers in Press, December 7, 2010, DOI 10.1074/jbc.M110.160713

Łukasz Jaremko[‡§1], Mariusz Jaremko[‡1], Imadeldin Elfaki[¶2], Jonathan W. Mueller[¶], Andrzej Ejchart[‡], Peter Bayer[¶3], and Igor Zhukov[‡‖4]**

*From the [‡]Institute of Biochemistry and Biophysics, Polish Academy of Sciences, Pawińskiego 5a, 02-106 Warsaw, Poland, the [¶]Institute for Structural and Medicinal Biochemistry, Center for Medical Biotechnology, ZMB, University of Duisburg-Essen, Universitaetstrasse 2, 45117 Essen, Germany, the [‖]Slovenian NMR Centre, National Institute of Chemistry, Hajdrihova 19, SI-1001 Ljubljana, Slovenia, the [§]Department of Chemistry, University of Warsaw, Pasteura 1, 02-093 Warsaw, Poland, and the **EN-FIST Center of Excellence, Dunajska 156, SI-1000 Ljubljana, Slovenia*

Parvulins are a group of peptidyl-prolyl isomerases (PPIases) responsible for important biological processes in all kingdoms of life. The PinA protein from the psychrophilic archaeon *Cenarchaeum symbiosum* is a parvulin-like PPIase. Due to its striking similarity to the human parvulins Pin1 and Par14, PinA constitutes an interesting subject for structural and functional studies. Here, we present the first high resolution NMR structure of an archaeal parvulin, PinA, based on 1798 conformational restraints. Structure calculation yields an ensemble of 20 convergent low energy structures with a backbone r.m.s.d. value of 0.6 Å within the secondary structure elements. The overall fold of PinA comprises the β-α_3-β-α-β_2 fold typical for all parvulin structures known so far, but with helix III being a short 3_{10}-helix. A detailed comparison of this high resolution structure of the first archaeal PinA protein with bacterial and eukaryotic parvulin PPIase structures reveals an atypically large catalytic binding site. This feature provides an explanation for cold-adapted protein function. Moreover, the residues in and around 3_{10}-helix III exhibit strong intramolecular dynamics on a microsecond to millisecond timescale and display structural heterogeneity within the NMR ensemble. A putative peptide ligand was found for PinA by phage display and was used for ^{1}H-^{15}N-HSQC titrations. Again, the flexible region around 3_{10}-helix III as well as residues of the peptide binding pocket showed the strongest chemical shift perturbations upon peptide binding. The local flexibility of this region also was modulated by ligand binding. A glycine and two positively charged residues are conserved in most parvulin proteins in this flexible loop region, which may be of general functional importance for parvulin-type PPIases.

Peptidyl-prolyl isomerases (PPIases)[5] catalyze the *cis*/*trans* rotation around the Xaa-Pro peptide bonds in target proteins. Pin proteins are small parvulin-type PPIases found in bacteria and all eukaryotes (1) and are involved in key steps of cell cycle regulation and protein quality control. This latter function relates parvulin proteins to folding disorders in human brain tissues such as Alzheimer and Parkinson diseases (2, 3). Very little is known about the archaeal members of this highly conserved protein family (4).

The genome of the psychrophilic archaeon *Cenarchaeum symbiosum* (5, 6) living in association with the marine sponge *Axinella mexicana* encodes a small protein isomerase (PinA), the first archaeal member of the parvulin PPIase family. The symbiotic archaeon *C. symbiosum* belongs to a large group of marine Archaea that eluded cultivation (7). It was initially classified as a member of the phylum of Crenarchaeota, but its optimal growth temperature at 10 °C differed strongly from the ones of any other cultivated member of that phylum (5). Recently, this species was grouped into a new deep-branching archaeal phylum, Thaumarchaeota (8).

There is nothing yet known about cold-optimized parvulins or about archaeal Pin proteins in general but only the PinA protein sequence from *C. symbiosum*. This protein comprises 92 amino acids without N- or C-terminal extensions to its PPIase domain similar to *Escherichia coli* Par10. Such extensions are found in eukaryotic parvulins or bacterial members of the SurA/PrsA-type (1, 9, 10). As seen in the alignment of several parvulins (Fig. 1), PinA does not contain an extended phosphoryl-binding loop typical for Ser(P)/Thr(P)-Pro specific PPIases such as human Pin1 (11, 12).

Though the function of this conserved protein within the psychrophilic endosymbiont is not known, it is tempting to

* This work was supported in part by Polish Ministry of Science and Higher Education Grant N301 07131/2159, Slovenian Research Agency Grant P1-0242-0104 (to I. Z.), Polish Ministry of Science and Higher Education Iuventus Plus program (project nr IP2010014570, to L. J.) .

⌘ *Author's Choice*—Final version full access.

[S] The on-line version of this article (available at http://www.jbc.org) contains supplemental Table 1 and Figs. S10–S13.

The atomic coordinates and structure factors (code 2RQS) have been deposited in the Protein Data Bank, Research Collaboratory for Structural Bioinformatics, Rutgers University, New Brunswick, NJ (http://www.rcsb.org/).

[1] Both authors contributed equally in this work.

[2] Fellow of Deutscher Akademischer Austauschdienst.

[3] To whom correspondence may be addressed. Tel.: 49-201-183-4677; Fax: 49-201-183-4188; E-mail: peter.bayer@uni-due.de.

[4] To whom correspondence may be addressed. Tel.: 386-1-476-0311; Fax: 386-1-476-0300; E-mail: igor.zhukov@ki.si.

[5] The abbreviations used are: PPIase, peptidyl-prolyl isomerase; r.m.s.d., root mean square deviation; HSQC, heteronuclear single-quantum correlation spectroscopy; *Cs*PinA, PinA protein from *C. symbiosum*; PDB, Protein Data Bank; BMRB, Biological Magnetic Resonance Bank; TOCSY, total correlated spectroscopy; T, Tesla; FKBP, FK506-binding protein.

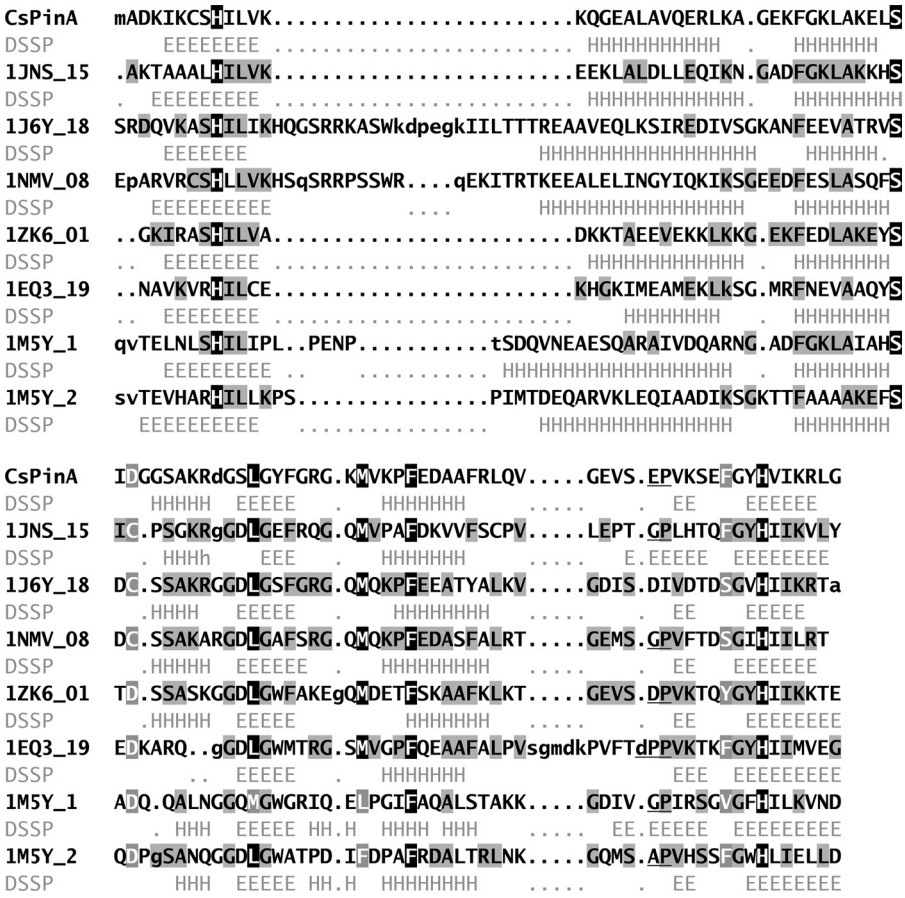

FIGURE 1. **Alignment of parvulin sequences from different organisms.** The available structures of parvulins were aligned onto the *Cs*PinA structure using DaliLite (50). Therefore, representative structures were chosen by NMRCLUST (51) and indicated within the alignment. For the loop region of 1J6Y and 1M5Y, an additional alignment on 1NMV_08 was used. Aligned residues are written as *uppercase letters*. Structures represent: 1JNS, *E. coli* Par10; 1J6Y, *Arabidopsis thaliana* Pin1; 1NMV, human Pin1; 1ZK6, *B. subtilis* PrsA; 1EQ3, human Par14; The structure of *E. coli* SurA contains two PPIase domains and 1M5Y_1 and 1M5Y_2 denote the N-terminal and C-terminal PPIase domain, respectively. Information for α-helical and β-sheet conformations from the PDB codes is given in *light gray below* the protein sequences. Residues believed to be important for PPIase activity are labeled in *white* and highlighted in *black* when conserved in most parvulins; otherwise, residues are colored *gray*. Other conserved residues relative to CsPinA are highlighted in *gray*. 1NMV and 1J6Y contain an extended N-terminal loop typical for phosphorylation-specific PPIases. A C-terminal loop specific for eukaryotic parvulins is contained in the 1EQ3 sequence. The Xaa-Pro motif conserved in many parvulins is *underlined*.

assume a role in cold adaptation like that seen with the FKBP-type PPIase in the psychrotrophic bacterium *Shewanella* (13). As a bacterium living at ambient temperatures, *E. coli* displays a cold shock response. Its ribosome-associated cold shock response protein YfiA inhibits translation at temperatures lower than 16 °C (14, 15). Enzymatically active PPIases should be highly important for the cold-loving archaeon *C. symbiosum* as the rates for the catalyzed and spontaneous *cis/trans* isomerization differ dramatically at lower temperatures (4). Of note, the *C. symbiosum* genome only contains two cyclophilins (RefSeq accession nos. YP_876752 and YP_876758), one FK506-binding protein (FKBP) (YP_876474), and the parvulin PinA under study. This is in stark contrast to the PPIase repertoire of *E. coli* with a total of eight PPIase genes.[6] Instead of facilitating the Xaa-Pro bond rotation at low temperatures, PPIases with little isomerization activity can function as binding modules for important peptidic structures or play as yet unknown cellular functions (1).

The current work aims to understand the first member of archaeal parvulins in terms of structure and dynamics as well as interaction with a ligand. We report the first high resolution structure of an archaeal parvulin, PinA, from the cold-loving archaeon *C. symbiosum*. The putative peptide binding site is clearly larger than that of any eukaryotic or bacterial parvulins known so far. Backbone dynamics studies indicate amino acids in and around 3_{10}-helix III to be significantly more flexible than those in the rest of the protein. A potential ligand for PinA was derived from phage display and binding involved residues Ser^{44}, Gly^{55}, Gly^{57}, Lys^{58}, Val^{60}, and Phe^{83} located around 3_{10}-helix III and the catalytic binding pocket. Considering that *C. symbiosum* has fewer PPIases than *E. coli*, our study represents a step forward in explaining the molecular basis of cold adaptation of *cis/trans* isomerization in psychrophilic Archaea. Moreover, the flexible loop contributing to ligand binding might be a general feature in all parvulins known to date.

EXPERIMENTAL PROCEDURES

Protein Expression and Purification—A coding sequence of the PinA protein from *C. symbiosum* (SwissProt database no.

[6] C. Lederer, personal communication.

O74049; RefSeq accession no. YP_876111) with *E. coli* adapted codon usage was synthesized (Entelechon, Regensburg, Germany) and BamHI/EcoRI cloned into a modified pET41 expression vector with GST fusion and a PreScission protease cleavage site (16), followed by expression in *E. coli* Rosetta and purification upon cell disruption by GSH affinity chromatography. The GST fusion was cleaved off by PreScission protease digestion and removed by size exclusion chromatography on a Superdex75 column. The same protocol was used to purify isotopically labeled PinA protein grown in M9 minimal medium with addition of $^{15}NH_4Cl$ and/or [U-^{13}C]glucose.

NMR Spectroscopy and Resonance Assignment—Samples of ^{13}C,^{15}N-double labeled *Cs*PinA were prepared by dissolving 0.8 mM protein in 50 mM Tris, pH 7.5, 50 mM NaCl. All spectra were recorded at 289 K on a Varian VNMRS 800 NMR spectrometer (Varian, Inc.) equipped with four channels, *z* axis pulsed field gradient unit and triple ($^1H/^{13}C/^{15}N$) cryogenic probe head with inverse detection. Heteronuclear NMR data were acquired using the States-TPPI quadrature method (17) followed by sensitivity enhanced detection (18). All chemical shifts are reported relative to 4,4-dimethyl-4-silapentane-1-sulfonic acid (DSS) as external reference. Acquired spectra were processed with NMRPipe (19) and analyzed using Sparky.

Sequence-specific assignments of backbone ^1H, ^{13}C, and ^{15}N resonances were obtained by analyzing three-dimensional heteronuclear HNCACB, CBCA(CO)NH, HNCA, HN(CO)CA, and HNCO spectra by standard methods (20) and confirmed by analyzing a ^{15}N-edited NOESY-HSQC spectrum. The ^1H and ^{13}C resonances in aliphatic side chains were assigned based on heteronuclear two-dimensional ^1H-^{13}C-HSQC, three-dimensional C(CO)NH, H(CCO)NH, and HCCH-TOCSY experiments. Aromatic side chain $^{13}C\delta$, $^{13}C\epsilon$, and $^{13}C\zeta$ resonances were assigned from two-dimensional ^1H-^{13}C-HSQC with tuned offset, spectral widths, and ^1H-^{13}C couplings to aromatic carbons, and three-dimensional ^{13}C-edited NOESY-HSQC spectra.

Structure Calculation—Distance constraints were derived from three NOESY spectra; the three-dimensional ^{15}N-edited NOESY-HSQC spectrum was recorded with a mixing time of 150 ms and two three-dimensional ^{13}C-edited NOESY-HSQC data sets with parameters tuned into either aliphatic or aromatic regions were acquired with a mixing time of 90 ms. The initial structure calculations were performed by CYANA (21) following the automated NOE assignment procedure (22). Stereospecific assignments for 92 chiral groups in side chains were derived by the program GLOMSA (23) included in CYANA software. Further structural calculations were performed in the CNS program (version 1.2) (24). Additionally, 76 distance constraints for 38 hydrogen bonds were defined as r_{HN-O} = 1.5–2.8 Å and r_{N-O} = 2.4–3.5 Å and included for structure calculations at final refining stage. Secondary structure was defined for PinA on the basis of $^2J_{N(i)C\alpha(i-1)}$ couplings, which are in good agreement with predicted secondary structure deduced from ^1H, ^{13}C, and ^{15}N chemical shifts using TALOS+ software (25). Analyzing experimental *J* couplings yield 70 restraints for ψ backbone torsion angles defined as $\psi = -40 \pm 40$ degrees (37 restraints), and $\psi = 140 \pm 40$ degrees (33 restraints) for α-helices and β-sheets, respectively. Finally, 20 structures of 200 calculated were selected according to lowest energy and deposited in the Protein Data Bank (PDB code 2RQS). Due to the five additional residues GPMGS remaining at the N terminus after PreScission protease cleavage, numbering in that PDB file has an offset of five relative to all numbering in the article. Quality of the ensemble was analyzed with PROCHECK-NMR (26) and WhatIf (27). Figures were generated with MOLMOL (28) or Chimera (29).

Relaxation Measurements—The ^{15}N longitudinal (R_1) and transverse (R_2) relaxation rates were measured at 289 K on Varian Unity+ 500 and Varian VNMRS 700 NMR spectrometers at 11.7 and 16.1 T, respectively. Both spectrometers were equipped with three channels (^1H, ^{13}C, ^{15}N), inverse probe heads, and a gradient unit. Relaxation rates were measured using pulse sequences included in BioPack (Varian, Inc.) with an optional measurement of either R_1 or R_2 relaxation on ^{15}N nuclei. Ten evolution times 10, 90, 170, 290, 410, 550, 690, 850, 1010, and 1250 ms were used in the ^{15}N R_1 experiments. The ^{15}N R_2 experiments were performed with eight evolution times 10, 30, 50, 90, 130, 170, 210, and 250 ms. The Carr-Parcell-Meiboom-Gill pulse train with a refocusing time of 650 μs was used in this case. The cross-correlation effect was suppressed by using π (^1H) pulses every 5 or 10 ms in R_1 and R_2 measurements, respectively (18). A relaxation delay of 3.0 s was employed in both experiments. R_1 and R_2 relaxation rates were calculated using two parameter, nonlinear least-square fit of cross-peak heights to a single exponential decay. Accuracies of R1 and R2 rates were determined from variance-covariance matrices. The {^1H}-^{15}N NOE were obtained from ratios of intensity cross-peaks in spectra with and without saturation and were also measured with a pulse sequence included in BioPack (Varian, Inc.). The relaxation delay of 8 s and a 3-s saturation delay were employed for recording these spectra. Experimental errors in {^1H}-^{15}N NOE were evaluated as described in (30).

Analysis of Relaxation Data—Relaxation data for PinA protein were analyzed using the model-free approach (31) combined with axially anisotropic overall molecular tumbling (32). Four global parameters $D_{\|}$, $D_{\perp}$, θ, and φ, denote parallel and perpendicular components of the rotational diffusion tensor and direction of unique axis of the diffusion tensor relative to the molecule fixed coordinate system, respectively. Three local, residue-specific parameters comprise a generalized order parameter *S*, which is a measure of the degree of spatial restriction of the motion, an effective correlation time τ_{int} corresponding to the rate of this motion, and R_{ex} describing conformational exchange contribution to R_2 resulting from the dynamic processes on a microsecond to millisecond time scale (33). All model parameters were determined simultaneously from the relaxation data and known orientations of N–H bonds calculated from the atomic coordinates of the NMR-derived structure of PinA protein. The least-squares procedure used to optimize model parameters consisted of a minimization through a grid search of the appropriate target functions using a Fortran routine written in-house. Model

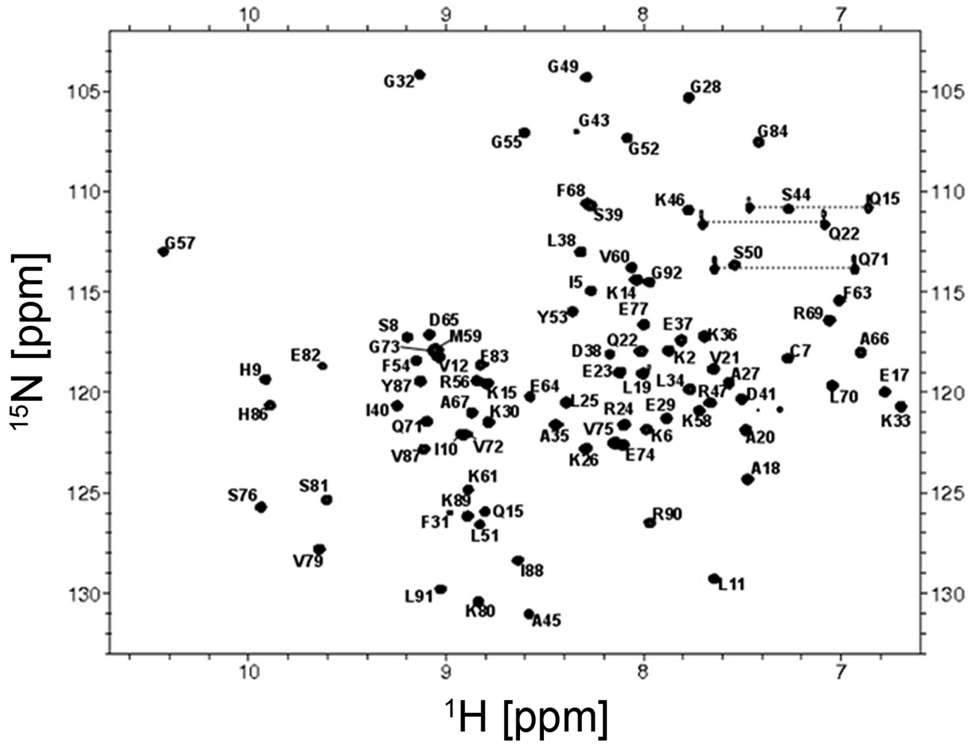

FIGURE 2. **Two-dimensional ^{1}H-^{15}N-HSQC spectrum of PinA recorded at 289 K on a Varian VNMRS 800 NMR spectrometer.** Obtained sequential assignments are indicated by the one-letter amino acid code and residue number.

parameter uncertainties derived in the minimization of target function were obtained as S.D. from 200 Monte Carlo simulations. The values of N–H distance, $r_{NH} = 0.103$ nm and ^{15}N chemical-shift anisotropy $\Delta\sigma = -160$ ppm were used in our calculations.

Phage Display and PinA Peptide Titration Experiments—Purified PinA protein was diluted in 0.1 M $NaHCO_3$, pH 8.6, to 0.1 mg/ml and immobilized on Petri dishes. Unbound protein was removed, and the plate was blocked with 5 mg/ml BSA in 0.1 M $NaHCO_3$, pH 8.6. A 7-mer M13 phage display peptide library (New England Biolabs) was used according to the manufacturer's protocol for three rounds of panning with increasing concentrations of Tween 20 (0.1% to 0.5%) within the washing buffer (Tween 20-containing Tris-buffered saline). Bound phages were eluted with 0.2 M glycine, pH 2.2. Following the third round of panning, clonal phage DNA was isolated and sequenced.

7-mer sequences that have been obtained several times were commercially synthesized at ChemCube (Bochum, Germany). Titration experiments were performed as series two-dimensional ^{1}H-^{15}N-HSQC spectra on a Varian Unity+ 500 NMR spectrometer at 283 K on samples containing 0.4 mM ^{13}C,^{15}N-doubly labeled protein in 50 mM Tris, pH 7.4, 50 mM NaCl, with 10% D_2O. Protein-peptide complexes were obtained by the addition of an equivalent amount of 6 mM stock solution prepared in the same buffer and pH; pH was additionally checked after titration. Spectra for four PinA-HQSPWHH ratios corresponding to 1:0, 1:1, 1:4, and 1:8 were acquired (supplemental Fig. S12). Chemical shift differences of backbone ^{1}H and ^{15}N were calculated according to Equation 1 (34).

$$\Delta\delta\ (\text{ppm}) = \sqrt{\Delta\delta(^{1}\text{H})^2 + 0.154\Delta\delta(^{15}\text{N})^2} \qquad \text{(Eq. 1)}$$

Dynamics measurements of the protein-peptide complex were performed as described above with an 0.8 mM protein sample and 7.6 mM HQSPWHH peptide (1:9.5 ratio) in the same buffer. Eight points for R_2 and 10 points for R_1 were collected and analyzed as described above.

RESULTS

Sequence-specific Resonance Assignment—Sequence-specific assignment of backbone ^{1}H, ^{13}C, and ^{15}N resonances of PinA from *C. symbiosum* was obtained from analyzing triple-resonance HNCACB, CBCA(CO)NH, HNCO, HNCA, and HN(CO)CA spectra. Existing cross-peaks were confirmed using a ^{15}N-edited three-dimensional NOESY-HSQC spectrum recorded with a 150-ms mixing time. Assignments of aliphatic ^{1}H and ^{13}C resonances of the protein side chains were achieved on the basis of three-dimensional HBHA-(CO)NH, C(CO)NH-TOCSY, and HCCH-TOCSY experiments. More than 96% of all resonances could be assigned by this procedure with the exception of signals from aromatic side chains and from six N-terminal residues (Met^{1} to Asp^{3} as well as residual amino acids from the N-terminal extension). Finally, all obtained ^{1}H, ^{13}C, and ^{15}N chemical shifts for the PinA protein were deposited in the Biological Magnetic Resonance Bank (BMRB accession no. 11080). A fully assigned ^{1}H-^{15}N-HSQC spectrum is shown in Fig. 2.

Information about the redox state of the unique cysteine residue (Cys^{7}) in PinA was deduced from the chemical shift of its $^{13}C\beta$ nucleus (35). The obtained value for this $^{13}C\beta$ chemical shift was 33.6 ppm, clearly indicating a reduced state of this thiol group.

Secondary Structure—Known structures of parvulin-like PPIases from various prokaryotic and eukaryotic organisms typically exhibit a β-α_3-β-α-β_2 fold (1, 36, 37). In the case of the PinA protein from *C. symbiosum*, the existence of three α-helices and four β-strands were predicted from inspection of $^2J_{N(i)C\alpha(i-1)}$ couplings measured in a three-dimensional HNCO Cα-coupling experiment (38). The $^2J_{N(i)C\alpha(i-1)}$ scalar couplings are strongly correlated with the ψ backbone torsion angle of a preceding residue and could be used for secondary structure prediction in proteins (39, 40). The extended or helical conformation could be predicted from deviation of $^2J_{N(i)C\alpha(i-1)}$ scalar coupling constants from the delineation value of 7.2 Hz (39), taking into account the negative sign of this coupling (40). Evaluation of $^2J_{N(i)C\alpha(i-1)}$ couplings of *Cs*PinA confirms the existence of four β-sheets by a series of at least three residues with $^2J_{N(i)C\alpha(i-1)}$ values smaller than -7.2 Hz within the secondary structure elements (Lys^4–Lys^{13}, Tyr^{53}–Gly^{57}, Val^{75}–Ser^{81}, and Tyr^{85}–Leu^{91}).

At the same time, four regions forming α-helices were postulated on the basis of values higher than -7.2 Hz (Glu^{17}–Glu^{29}, Glu^{32}–Ser^{39}, Ser^{44}–Arg^{47}, and Phe^{63}–Leu^{70}). According to these data, the organization of the secondary structure elements of PinA could be described as a β-α_3-β-α-β_2 topology. This topology is in good agreement with the analysis of chemical shift data using the TALOS+ software (25), where backbone conformations for 78 of 94 residues were classified as "good." Nevertheless, the exact positions of α-helices and β-sheets were justified only after full analysis of NOE connectivities obtained from the three-dimensional ^{15}N-edited NOESY-HSQC spectrum. Three α-helices (Gln^{15}–Leu^{25}, Phe^{31}–Glu^{37}, and Lys^{61}–Ala^{66}) were confirmed on the basis of H_N-Hα (i, i+4) and (i, i+3) NOE contacts. The four β-sheets (Ile^5–Leu^{11}, Ser^{50}–Phe^{54}, Val^{79}–Ser^{81}, and Gly^{84}–Arg^{90}) were identified on the basis of HN-HN and HN-HA NOE contacts. Finally, the proposed α-helix III turned out to be a short one-turn 3_{10}-helix between Gly^{43} and Arg^{47}, as confirmed by H_N-Hα (i, i+2) NOE contacts.

Structure Calculations and Tertiary Structure of CsPinA Protein—The high resolution solution structure of PinA was determined with 1585 distance constraints (777 intraresidual and sequential, 294 short range, and 514 long range NOEs) and 175 restraints for backbone torsion angles using CNS software (version 1.2) (24). Moreover, 38 hydrogen bonds, which yielded an additional 76 distance constraints (r_{NH-O} 1.5–2.8 Å and r_{N-O} 2.5–3.5 Å), were defined on the basis of NOESY cross-peaks and the previously determined secondary structures that were introduced during the refinement procedure. The statistics of distance constraints and analysis of the NMR ensemble containing the 20 lowest energy structures of PinA protein are presented in Table 1; the ensemble was deposited in the Protein Data Bank (PDB code 2RQS).

The globular fold of the PinA protein from *C. symbiosum* exhibits a central four-stranded β-sheet motif wrapped around the C-terminal α-helix IV (Fig. 3*A*). Hydrophobic residues (Leu^{51}, Phe^{54}, and Ile^{92}) and the two histidines (His^9 and His^{86}) forming the hydrophobic core are located on the concave side of the β-sheet cluster. The other, convex side is defined by the hydrophilic residues Cys^7, Ser^8, Lys^{89}, and Arg^{90}.

TABLE 1
NMR constraints and structural statistic for the ensemble of the 20 lowest energy PinA conformers of *C. symbiosum*

NOE distance constraints[a]	1585	
Intraresidual and sequential ($\|i-j\| \geq 1$)	777	
Medium range ($1 < \|i-j\| < 5$)	294	
Long range ($\|i-j\| \geq 5$)	514	
Hydrogen bonds	38	
Restraints per residue	17.1	
Torsion angle constraints		
Backbone (φ/ψ)	70	
r.m.s.d. from idealized covalent geometry (±S.D.)		
Bonds (Å)	0.0020 ± 0.0001	0.0018
Angles	0.338 ± 0.005°	0.330°
Impropers	0.198 ± 0.010°	0.177°
Ramachandran plot (region 2–92)[b]		
Residues in most favored regions (%)	71.3 ± 3.4	78.8
Residues in additional allowed regions (%)	27.0 ± 3.4	32.5
Residues in generously allowed regions (%)	1.1 ± 1.1	3.8
Residues in disallowed regions	0.6 ± 1.0	0.0
r.m.s.d. to the mean structure (2–92) (Å)		
Ordered backbone atoms	0.62 ± 0.17	
Ordered heavy atoms	1.34 ± 0.15	
Equivalent x-ray resolution (2–92)	2.1 Å	
r.m.s. Z-scores[c]		
Bond lengths	1.035 ± 0.001	
Bond angles	0.287 ± 0.003	
ω angle restraints	0.157 ± 0.010	
Side chain planarity	0.081 ± 0.023	
Improper dihedral distribution	0.381 ± 0.019	
Inside/outside distribution	0.986 ± 0.018	

[a] None of the 20 structures had a distance violation more than 0.2 Å or a dihedral angle violation >5°.
[b] Quality of the ensemble consisting of the 20 lowest energy structures of PinA was checked by PROCHECK-NMR (version 3.4).
[c] Ensemble of structures was validated using WhatIf (27).

The determined three-dimensional fold is very similar to the other PPIase structures from various organisms known to date. An overlay of PinA with the structures of human Pin1, *E. coli* Par10 and *Bacillus subtilis* PrsA shows an r.m.s.d. over backbone heavy atoms of ~1.2 Å (Fig. 4). Residues that are postulated as important for catalyzing the Xaa-Pro peptide bond isomerization (His^9, Asp^{41}, Met^{59}, Phe^{63}, Phe^{83}, and His^{86}) are essentially at the same positions.

Conformation of a Conserved Xaa-Pro Peptide Bond—One intriguing structural question in parvulin-type PPIases surrounds the conformation of a conserved Xaa-Pro peptide bond within the catalytic domain. In *E. coli* Par10, the Gly^{76}–Pro^{77} bond has been reported to be in *cis* conformation (37) and the corresponding Asp^{113}–Pro^{114}–Pro^{115} in human Par14 was assigned a *cis* conformation for the Asp^{113}–Pro^{114} bond (36). Initially, $^{13}C_\beta$ and $^{13}C_\gamma$ chemical shift data for the two proline residues, Pro^{62} and Pro^{78} of *Cs*PinA, were used to determine the probability of *cis* conformation using the program PROMEGA (41), which uses both chemical shift data and sequence context for prediction. The *trans* conformation was postulated for both prolines in our structure. In the case of the Gly^{77}–Pro^{78}, the conserved Xaa-Pro bond in parvulins, the *trans* conformation was additionally validated by the analysis of three-dimensional NOESY-HSQC ^{13}C-edited spectra, where cross-peaks between Glu^{77} Hα and Pro^{78} Hδ as well as between Pro^{78} Hα and Val^{79} HN were clearly detected. This conformation is similar to the PrsA structures from *B. subtilis* (42), *Staphylococcus aureus* (43), and other parvulins. Our PROMEGA prediction for this conserved motif was then extended to all other parvulins whose chemical ^{1}H, ^{15}N, and ^{13}C

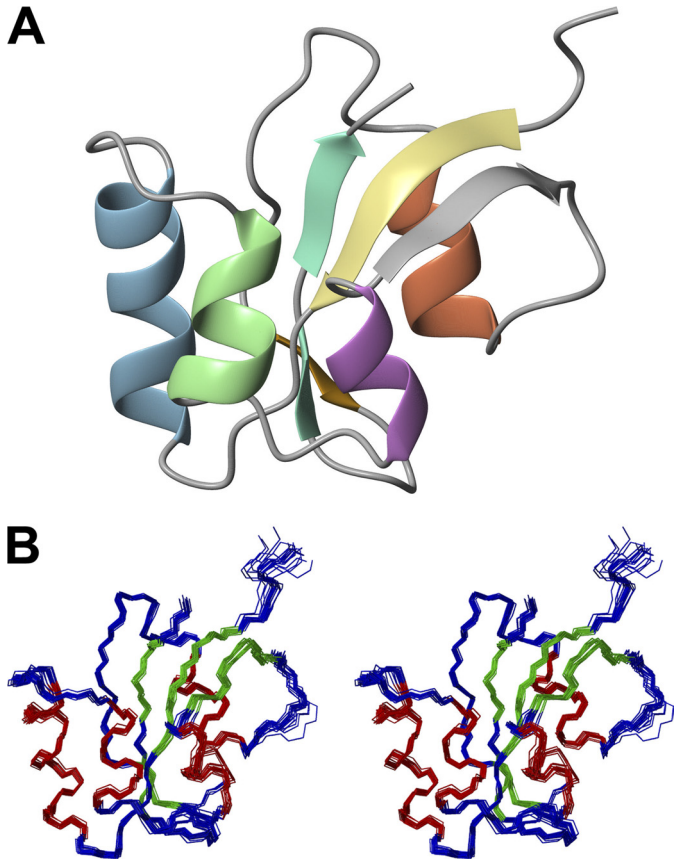

FIGURE 3. **NMR solution structure of the parvulin protein PinA from *C. symbiosum*.** Only the structured parts (residues 2–92) are shown. *A*, ribbon representation of PinA protein. Four helices and four β-sheets are presented by different colors demonstrating the globular β-α_3-β-α-β_2 fold characteristic for parvulins. *B*, stereo view of backbone ensemble of the 20 lowest energy structures. Residues in helical and extended conformation are shown in *red* and *green*, respectively.

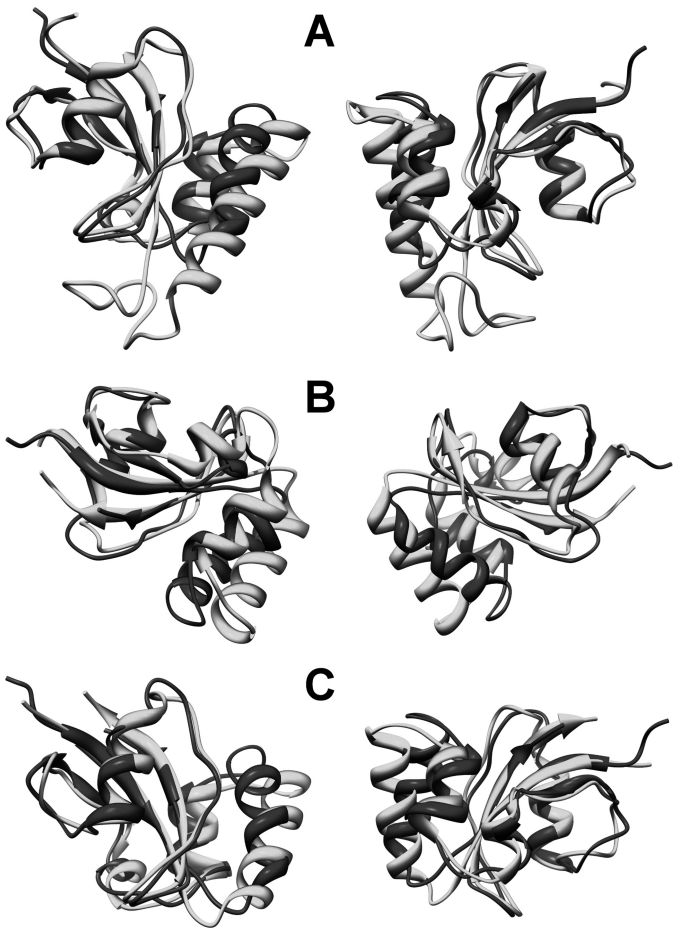

FIGURE 4. **Structural similarities between various parvulins.** Overlay of the PinA structure from *C. symbiosum* (*black*) with *Homo sapiens* Pin1 PPIase domain (*A*; PDB 1PIN), *E. coli* Par10 (*B*; PDB 1JNS), and *B. subtilis* PrsA (*C*; PDB 1ZK6).

shifts were available in the BMRB. The probabilities for the conserved Xaa–Pro bond to be in *cis* conformation are listed in Table 2 for six of them. Following this prediction, a *cis* Xaa–Pro bond is found only in *E. coli* Par10 and human Par14 (see also supplemental Fig. S11).

Backbone Dynamics of PinA from Relaxation Data—To study the global and local backbone dynamics of *Cs*PinA, ^{15}N relaxation rates, R_1 and R_2, were determined at two magnetic fields, 11.7 and 16.4 T. Additionally, {^{1}H}-^{15}N NOEs were measured at the lower magnetic field. Relaxation data were obtained for 79 backbone amide groups. Missing data comprise two prolines (Pro^{62} and Pro^{78}), N-terminal residues Met^1–Asp^3, together with residues from the N-terminal extension experiencing fast exchange of their H_N protons with water as well as several residues scattered along the polypeptide chain with strongly superposed cross-peaks. These data are shown in Fig. 5.

The inertia tensor of the PinA protein was calculated from the PDB coordinates. Its principal value ratios were 1.51:1.66:1.00, allowing the approximation of the protein molecule as a prolate ellipsoid. Rotational diffusion constants and local model parameters were determined after rejection of doubtful R_1 data at 16.1 T for Lys^4 and Ala^{45}. The overall molecular

TABLE 2

Probability (P_{cis}) for a Xaa-Pro peptide bond being in *cis* conformation calculated by the program PROMEGA

Gly^{75}–Pro^{76} and Pro114-Pro115 with a high probability for the *cis* conformation are highlighted in *bold*.

Protein	Peptide bond	P_{cis}
E. coli Par10 (1JNS)[a]	Glu^{72}–Pro^{73}	0.124
	Gly^{75}–Pro^{76}	**0.987**
H. sapiens Par14 (1EQ3)[b]	Asp^{113}–Pro^{114}	0.092
	Pro^{114}–Pro^{115}	**0.991**
B. substitilis PrsA (1ZK6)[c]	Asp^{77}–Pro^{78}	0.000
Mycoplasma genitalium PpiD (1HXV)[d]	Lys^{101}–Pro^{102}	0.051
C. symbiosum PinA (2RQS)[e]	Glu^{82}–Pro^{83}	0.022
H. sapiens Pin1 (1PIN)[f]	Lys^{152}–Pro^{153}	0.000
	Gly^{168}–Pro^{169}	0.056

[a] BMRB accession no. 5225.
[b] BMRB accession no. 4768.
[c] BMRB accession no. 6601.
[d] BMRB accession no. 4953.
[e] BMRB accession no. 11080.
[f] BMRB accession no. 5305.

diffusion constants were: $D_{\parallel} = (4.09 \pm 0.08)\ 10^7\ s^{-1}$ and $D_{\perp} = (1.70 \pm 0.04)\ 10^7\ s^{-1}$.

Anisotropy of the overall motion is considerable with the anisotropy ratio $D_{\parallel}/D_{\perp} = 2.41 \pm 0.07$, indicating a substantial deviation of the protein structure from a spherical shape. An effective correlation time of $\tau_R = 1/(2D_{\parallel} + 4D_{\perp}) = 6.7 \pm 0.1$ ns (32) fits well with the value expected for a 97-residue protein (44, 45).

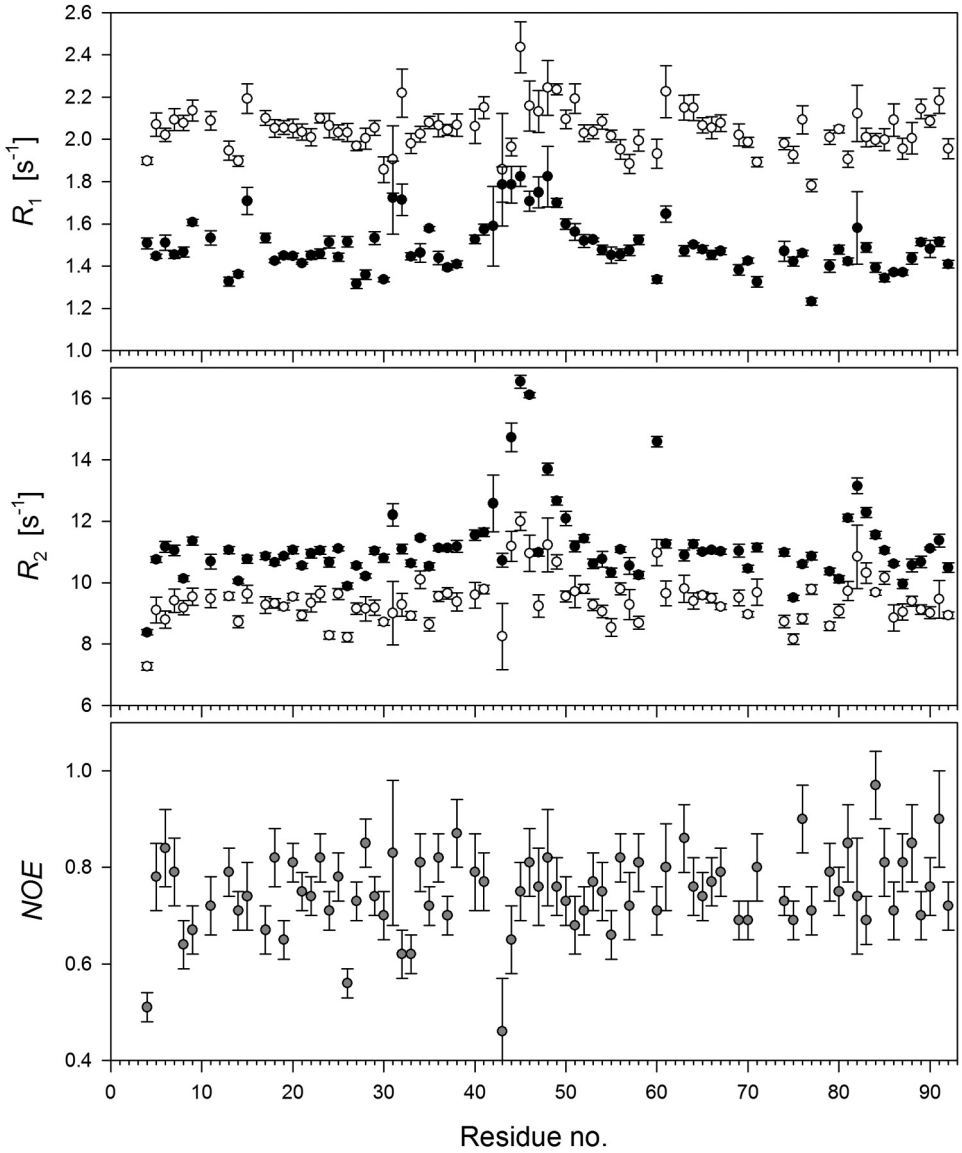

FIGURE 5. **Relaxation data for backbone amide ^{15}N nuclei.** R_1, R_2, and {^{1}H}-^{15}N NOE of *Cs*PinA protein at 11.7 T (*open circles*) and 16.4 T (*closed circles*), respectively. The mean values for R_1 rates are 2.05 s^{-1} and 1.50 s^{-1} at 11.7 and 16.4 T, respectively. The mean values for R_2 rates are 9.40 s^{-1} and 11.21 s^{-1} at 11.7 and 16.4 T, respectively. Finally, the {^{1}H}-^{15}N NOE mean value was 0.75 at 11.7 T. For definition of the *error bars*, please refer to the "Relaxation Measurements" under "Experimental Procedures."

All determined values of local parameters, S^2 and R_{ex}, are included in the BMRB deposition (BMRB accession no. 11080) and are shown in Fig. 6. Correlation times for internal motions, τ_{int}, are very sensitive to experimental errors resulting in large inaccuracies, as often observed (46). Therefore, their values are hardly informative and not presented here.

Fast and simple identification of the residues undergoing conformational exchange slower than the overall molecular tumbling can be derived from larger than average values of R_1R_2 product (47). It is superior to the R_1/R_2 ratio, which is prone to errors in the case of anisotropic overall tumbling. R_1R_2 values calculated from relaxation rates determined at 16.4 T are shown in Fig. 6. On the other hand, smaller than average values of the R_1R_2 product indicate residues with increased mobility on a subnanosecond timescale. It has to be stressed that R_1R_2 values cannot be used uncritically instead of full analysis of all available relaxation data. Residues undergoing both fast and slow motions can display average R_1R_2 product values due to mutual cancellation of the two opposite effects.

Residues with larger R_1R_2 values also displayed elevated R_{ex} values, unequivocally pointing to increased mobility on a microsecond to millisecond time scale. Large R_{ex} values for Gly^{42}, Gly^{43}, Ser^{44}, Ala^{45}, Lys^{46}, Asp^{48}, and Gly^{49} at 11.7 T were equal to 1.8 ± 0.7 s^{-1}, 1.7 ± 0.4 s^{-1}, 3.5 ± 0.2 s^{-1}, 3.7 ± 0.3 s^{-1}, 3.5 ± 0.2 s^{-1}, 1.7 ± 0.6 s^{-1}, and 2.1 ± 0.1 s^{-1}, respectively. Residues Gly^{43}–Arg^{47} constitute the short one turn 3_{10}-helix III sandwiched between the two nonstructured loops. Analysis of the ensemble of the 20 lowest energy structures of the protein confirms a relatively high r.m.s.d. value of 0.35 ± 0.22 Å for this 3_{10}-helix relative to the other secondary structure elements (0.09 ± 0.06 Å for β-sheet I and 0.18 ± 0.07 Å for α-helix I). This structural heterogeneity is in agreement with the flexibility detected

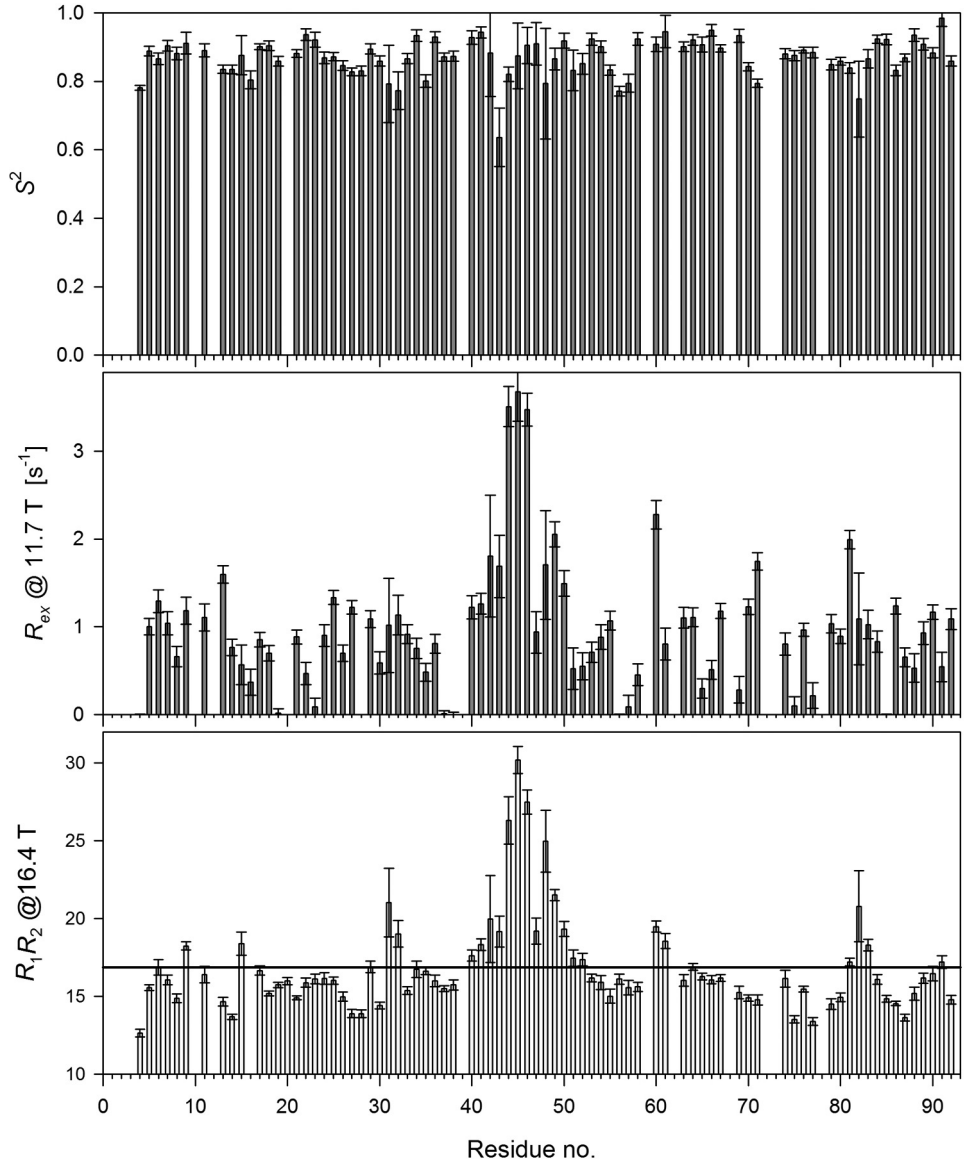

FIGURE 6. **Model-free approach parameters, S^2 (*top*) and R_{ex} at 11. 7 T (*middle*) and R_1R_2 product values at 16.4 T (*bottom*) for *Cs*PinA protein.** Note the different R_{ex} and R_1R_2 values for the region from amino acids Ser[44] to Gly[49]. For definition of the *error bars*, please refer to "Analysis of Relaxation Data" under "Experimental Procedures."

in this region. Other residues displaying chemical exchange, Val[60] (2.3 ± 0.2 s^{-1}), Gln[71] (1.7 ± 0.1 s^{-1}), and Ser[81] (2.0 ± 0.1 s^{-1}), are located in unstructured parts of the molecule.

The weighted mean of the S^2 parameter for residues forming three α-helices and four β-sheets (0.88 ± 0.04) does not differ from the weighted mean calculated for all residues (0.87 ± 0.05) within the accuracy limit. Residues involved in secondary structure elements, except 3_{10}-helix, are very rigid; they exhibit no significant internal mobility. Several residues dispersed along the polypeptide chain display relatively small values of the S^2 parameter, which are usually associated with their high S.D. due to low accuracy of experimental data and cannot be attributed to the increased mobility on a fast timescale. Lys[4] located at the flexible N terminus (S^2 = 0.78 ± 0.1) is a unique prominent exception.

Phage Display and ^{1}H-^{15}N-HSQC Titrations Identify Peptide HQSPWHH as a Ligand of PinA—To identify interacting partners of PinA from the archaeon *C. symbiosum* that cannot be cultivated, we screened a 7-mer peptide phage display using our recombinant protein as bait. The heptamer sequence HQSPWHH was selected several times during screening and hence was obtained as a peptide for titration purposes. ^{1}H-^{15}N-HSQC spectra for four protein:peptide ratios (1:0, 1:1, 1:4, and 1:8) were recorded for *Cs*PinA and the HQSPWHH peptide. A plot of the chemical shift perturbation shows that the selected HQSPWHH peptide has an affinity in the high micromolar/low millimolar range. Structural mapping of the chemical shift perturbation (supplemental Fig. S12) demonstrates that peptide binding primarily affects residues of the catalytic binding pocket (Gly[57], Lys[58], Val[60], and Phe[83]) and within the 3_{10}-helix III (Gly[42] and Ser[44]). Monitoring

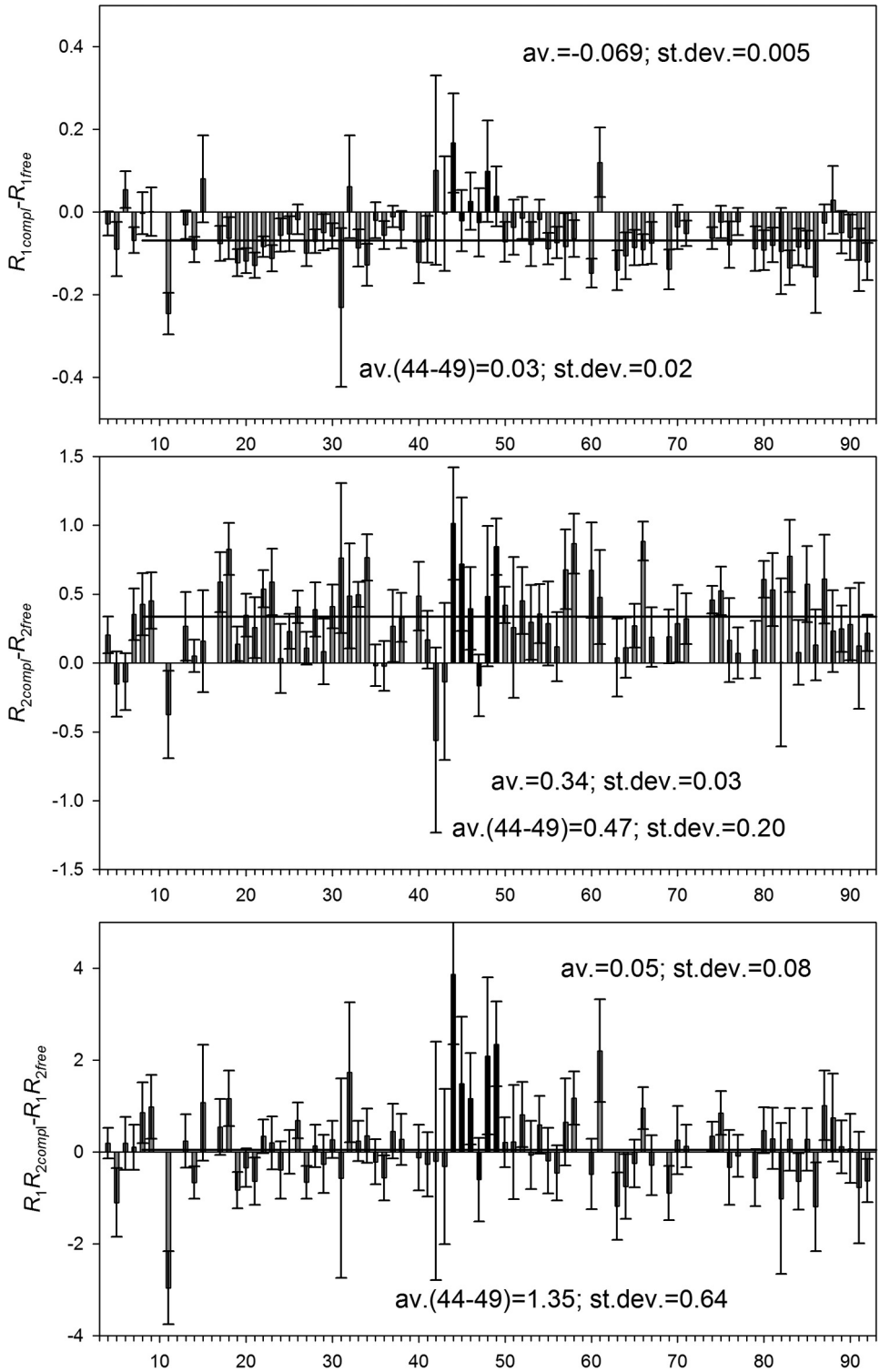

FIGURE 7. **Changes in dynamics upon binding of the peptide HQSPWHH.** Differences for the R_1 and R_2 relaxation parameters and the R_1R_2 product are shown for free PinA protein and complexed to the peptide HQSPWHH. Formal statistical analysis includes averaging over all amino acids as well as the flexible region from Ser[44] to Gly[49] (*black bars*). *av.*, average; *st. dev.*, S.D. For definition of the *error bars*, please refer to "Analysis of Relaxation Data" under "Methods."

HQSPWHH peptide binding with ^{1}H-^{13}C correlation spectra allowed the detection of chemical shift changes for the $C_{\epsilon 1}$/$H_{\epsilon 1}$ correlation of His[9] and His[86] within the PinA protein, residues that are part of the substrate binding pocket (supplemental Fig. S13).

This peptide ligand for CsPinA then allowed the investigation of protein dynamics and their changes upon ligand binding. Therefore, R_1 and R_2 relaxation parameters were again measured for ^{15}N amide groups in the presence and absence of the HQSPWHH peptide (Fig. 7). Clearly, the region from Ala[44] to

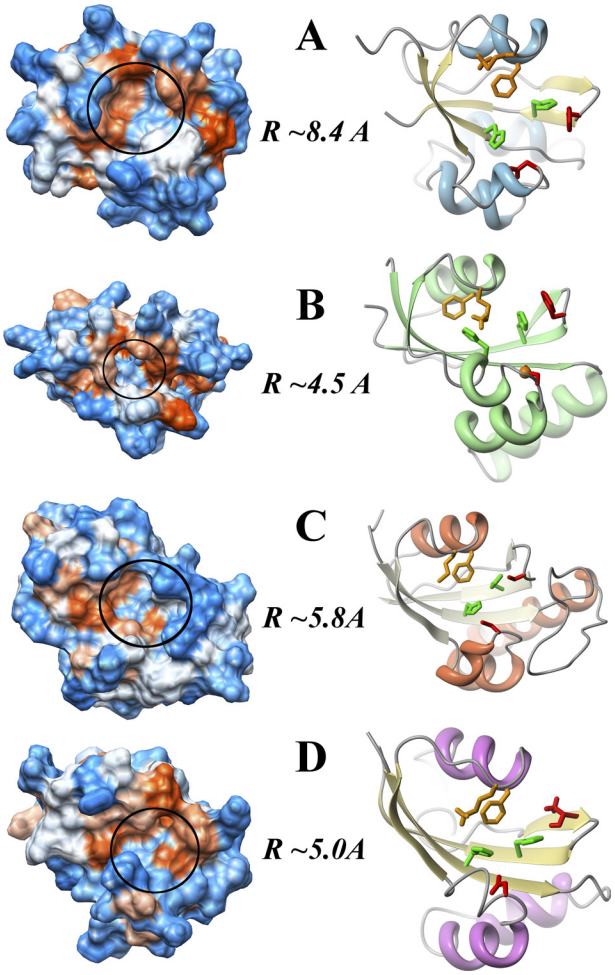

FIGURE 8. **The hydrophobicity surface of selected parvulins (*left*) together with their ribbon representations of secondary motifs (*right*).** The side chains for evolutionary conserved residues that are important for *cis/trans* isomerization are shown on the *right*. *Black circles* indicate opening of the catalytic substrate binding site. The radius of this binding pocket was calculated using MOLMOL (28) with an error of 0.4 Å. *C. symbiosum* PinA (PDB 2RQS; *A*), *E. coli* Par10 (PDB 1JNS; *B*), *H. sapiens* Pin1 (PDB 1PIN; *C*), and *H. sapiens* Par14 (PDB 1EQ3; *D*).

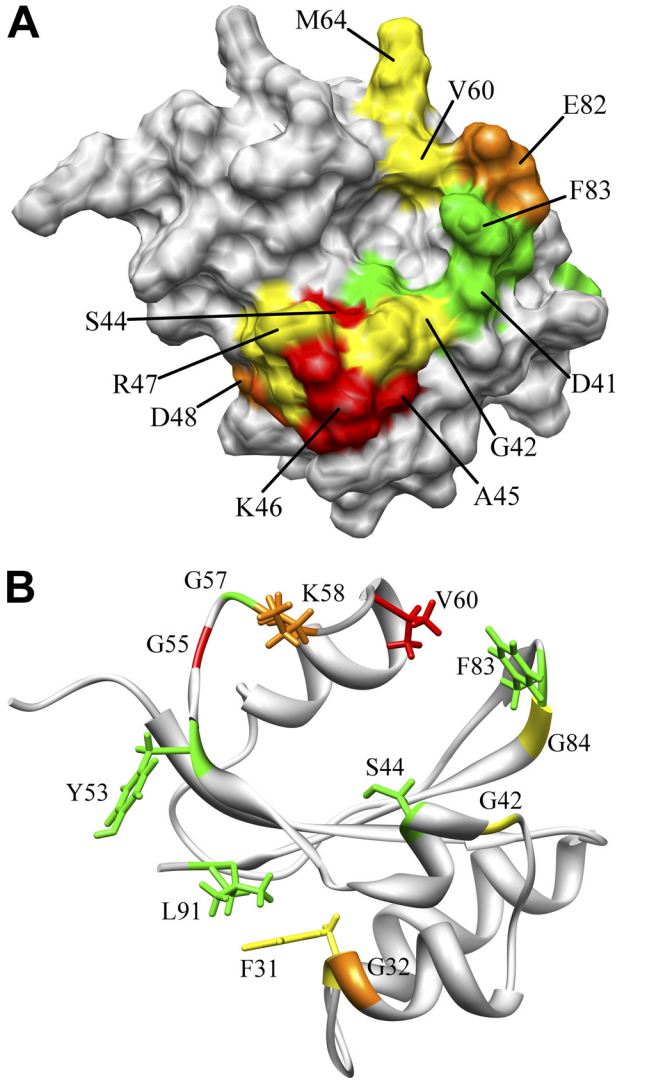

FIGURE 9. **Dynamic residues of the PinA protein and residues affected by ligand binding are found around the catalytic center.** *A*, mapping of residues exhibiting strong dynamics on the μs-ms time scale on the three-dimensional structure of PinA. The residues His[9], Gln[20], Phe[31], Gly[32], Asp[41]–Ser[50], Val[60], Lys[61], Glu[82], and Phe[83] are shown in *red*, *orange-red*, *orange*, and *yellow* depending on the intensity of their R_1R_2 product derived from ^{15}N relaxation data. *B*, residues demonstrating chemical shift perturbations larger than 0.022 ppm upon HQSPWHH peptide binding are shown in *red* (Gly[55], Val[60]), orange (Gly[32], Lys[58]), yellow (Phe[31], Gly[42], Gly[84]), and green (Ser[44], Gly[53], Gly[57], Phe[83], Lys[89]), respectively. See supplemental Fig. S12 for more information.

Gly[49] showed a different behavior from the rest of the protein, indicating increased mobility on a microsecond to millisecond time scale despite of strongly anisotropic overall tumbling.

DISCUSSION

The overall three-dimensional structure of the PinA protein from *C. symbiosum* is characterized by the typical parvulin-like β-α_3-β-α-β_2 fold (four α-helices exposed to the solvent and four β-sheets with a 3-4-1-2 strand order), classifying *Cs*PinA as a member of the FKBP-superfold family. Superpositions of backbone heavy atoms between the PPIase domain of human Pin1 (48), the *E. coli* Par10 (37) and *B. subtilis* PrsA (42) with the PinA as a reference molecule show r.m.s.d. values of 1.05, 1.22, and 1.09 Å, respectively. These values clearly indicate that parvulins are structurally and evolutionarily well conserved among different species. Moreover, the structural similarities dictate the geometry of the catalytic center, which remains the same among all known PPIases from different organisms. The residues that are strongly conserved and postulated as important for Xaa-Pro substrate binding, His[9], Asp[41], Met[59], Phe[63], Phe[83], and His[86], occupy essentially the same positions (Fig. 8). Nevertheless, there are some structural features occurring exclusively in cold-adapted parvulins that may be responsible for cold adaptation of parvulins from Thaumarchaeota.

An Unusually Large Catalytic Binding Pocket Is Observed in PinA from C. symbiosum—When comparing the structure of CsPinA with those of the other parvulins, it becomes evident that the hydrophobic catalytic center and its surrounding environment are remarkably different. Despite the structural build-up of the catalytic center that is essentially identical to other homologous parvulins, the accessibility of Xaa-Pro substrates to the active center in *Cs*PinA is dramatically different from other parvulins.

We analyzed the diameter of the entrance to the substrate binding pocket (Fig. 8). In the case of the archaeal PinA protein, the radius of the catalytic center is 8.4 ± 0.5 Å in size. For the atomic structures of other parvulins known to date, this parameter lies between 4.5 and 5.8 Å, irrespective of their different substrate specificities. A large substrate binding pocket may indicate a preference for bulky, hydrophobic residues similar to the substrate specificity of *E. coli* Par10, but even then, there is a significant difference between these two proteins. Enlarged catalytic clefts have been previously reported for other proteins of psychrophilic origin (49). In light of these data, the catalytic center of PinA from *C. symbiosum* can be regarded as an evolutionary adaptation of this protein for functioning in a cold environment.

Slow Molecular Dynamic Processes Are Especially Important for Protein-Substrate Binding—Molecular dynamics on microsecond to millisecond time scales (conformational exchange) is another important factor for protein-substrate interaction. The stretch of residues Gly^{42}–Gly^{49} as well as Val^{60}, Gln^{71}, and Ser^{80} showed significantly elevated R_{ex} values (Fig. 6). Out of these, Ser^{44}, Val^{60}, and Ser^{80} are located around the ligand binding site, which is conserved between different parvulins (Fig. 9). Our results extend former observations of some local flexibility in the helix III region of other parvulins. Elevated flexibility in this region was contained in the relaxation data reported for the PrsA parvulin from *S. aureus* (43). As a glycine and two positively charged residues within this loop are conserved in most parvulin proteins, this flexible loop may be of general importance for parvulin function.

Next, peptides were selected for PinA binding by phage display. This screening resulted only in relatively weak binders, which might indicate that PinA from *C. symbiosum* is an isomerase with little specificity for the primary sequence of its substrates. The peptide HQSPWHH was used for chemical shift perturbation studies with PinA. Interestingly, the residues most affected by ligand binding are located in a groove formed by helix II, β-sheet II, and the highly mobile short 3_{10}-helix III. Flexibility of this stretch of five residues within and around the short 3_{10}-helix III has not been reported previously for any other parvulin.

Conclusions—The high resolution three-dimensional structure of PinA from the psychrophilic archaeon *C. symbiosum* was determined from NMR data. Relative to other known parvulin structures, PinA has an atypically large catalytic binding site providing an explanation for cold-adapted protein function in Archaea. The structure of PinA is relatively rigid; only one stretch of residues comprising 3_{10}-helix III and the following turn displayed significant mobility on a microsecond to millisecond time scale and showed structural heterogeneity within the NMR ensemble. The peptide HQSPWHH was identified as a *Cs*PinA ligand and used for HSQC titrations and dynamics measurements of the complex. In addition to known residues involved in *cis*/*trans* isomerization, the flexible region around 3_{10}-helix III showed the strongest chemical shift perturbations and a change in flexibility upon peptide binding. The extraordinary flexibility of this region and its involvement in ligand binding has not previously been recognized for parvulin-type PPIases.

Acknowledgments—We thank Drs W. Kozminski, K. Kazimierczuk, and A. Zawadzka-Kazimierczuk (Chemistry Department, University of Warsaw) for technical assistance in recording and processing of three-dimensional HNCO $^{13}C\alpha$-coupled ultrahigh resolution NMR data sets. Christoph Lederer is acknowledged for searching a variety of genomes for PPIase genes, and Alma Rueppel performed excellent sample preparation. The measurements on the Varian VNMRS 700 NMR spectrometer were performed in the Structural Research Laboratory (Chemistry Department, University of Warsaw).

REFERENCES

1. Mueller, J. W., and Bayer, P. (2008) *Perspect. Medicin. Chem.* **2,** 11–20
2. Ryo, A., Togo, T., Nakai, T., Hirai, A., Nishi, M., Yamaguchi, A., Suzuki, K., Hirayasu, Y., Kobayashi, H., Perrem, K., Liou, Y. C., and Aoki, I. (2006) *J. Biol. Chem.* **281,** 4117–4125
3. Rudrabhatla, P., Zheng, Y. L., Amin, N. D., Kesavapany, S., Albers, W., and Pant, H. C. (2008) *J. Biol. Chem.* **283,** 26737–26747
4. Maruyama, T., Suzuki, R., and Furutani, M. (2004) *Front Biosci.* **9,** 1680–1720
5. Preston, C. M., Wu, K. Y., Molinski, T. F., and DeLong, E. F. (1996) *Proc. Natl. Acad. Sci. U.S.A.* **93,** 6241–6246
6. Hallam, S. J., Mincer, T. J., Schleper, C., Preston, C. M., Roberts, K., Richardson, P. M., and DeLong, E. F. (2006) *PLoS. Biol.* **4,** e95
7. Karner, M. B., DeLong, E. F., and Karl, D. M. (2001) *Nature* **409,** 507–510
8. Brochier-Armanet, C., Boussau, B., Gribaldo, S., and Forterre, P. (2008) *Nat. Rev. Microbiol.* **6,** 245–252
9. Mueller, J. W., Kessler, D., Neumann, D., Stratmann, T., Papatheodorou, P., Hartmann-Fatu, C., and Bayer, P. (2006) *BMC. Mol. Biol.* **7,** 9
10. Kessler, D., Papatheodorou, P., Stratmann, T., Dian, E. A., Hartmann-Fatu, C., Rassow, J., Bayer, P., and Mueller, J. W. (2007) *BMC Biol.* **5,** 37
11. Bayer, E., Goettsch, S., Mueller, J. W., Griewel, B., Guiberman, E., Mayr, L. M., and Bayer, P. (2003) *J. Biol. Chem.* **278,** 26183–26193
12. Yaffe, M. B., Schutkowski, M., Shen, M., Zhou, X. Z., Stukenberg, P. T., Rahfeld, J. U., Xu, J., Kuang, J., Kirschner, M. W., Fischer, G., Cantley, L. C., and Lu, K. P. (1997) *Science* **278,** 1957–1960
13. Suzuki, Y., Haruki, M., Takano, K., Morikawa, M., and Kanaya, S. (2004) *Eur. J. Biochem.* **271,** 1372–1381
14. Rak, A., Kalinin, A., Shcherbakov, D., and Bayer, P. (2002) *Biochem. Biophys. Res. Commun.* **299,** 710–714
15. Ye, K., Serganov, A., Hu, W., Garber, M., and Patel, D. J. (2002) *Eur. J. Biochem.* **269,** 5182–5191
16. Grum, D., van den Boom, J., Neumann, D., Matena, A., Link, N. M., and Mueller, J. W. (2010) *Biochem. Biophys. Res. Commun.* **395,** 420–425
17. Marion, D., Ikura, M., Tschudin, R., and Bax, A. (1989) *J. Magn. Reson.* **85,** 393–399
18. Kay, L. E., Nicholson, L. K., Delaglio, F., Bax, A., and Torchia, D. A. (1992) *J. Magn. Reson.* **97,** 359–375
19. Delaglio, F., Grzesiek, S., Vuister, G. W., Zhu, G., Pfeifer, J., and Bax, A. (1995) *J. Biomol. NMR* **6,** 277–293
20. Ikura, M., Kay, L. E., and Bax, A. (1990) *Biochemistry* **29,** 4659–4667
21. Güntert, P., Mumenthaler, C., and Wüthrich, K. (1997) *J. Mol. Biol.* **273,** 283–298
22. Herrmann, T., Güntert, P., and Wüthrich, K. (2002) *J. Mol. Biol.* **319,** 209–227
23. Güntert, P., Qian, Y. Q., Otting, G., Müller, M., Gehring, W., and Wüthrich, K. (1991) *J. Mol. Biol.* **217,** 531–540
24. Brunger, A. T. (2007) *Nat. Protoc.* **2,** 2728–2733
25. Shen, Y., Delaglio, F., Cornilescu, G., and Bax, A. (2009) *J. Biomol. NMR*

44, 213–223
26. Laskowski, R. A., Rullmannn, J. A., MacArthur, M. W., Kaptein, R., and Thornton, J. M. (1996) *J. Biomol. NMR* **8,** 477–486
27. Vriend, G. (1990) *J. Mol. Graph.* **8,** 52–56
28. Koradi, R., Billeter, M., and Wüthrich, K. (1996) *J. Mol. Graph.* **14,** 51–55
29. Pettersen, E. F., Goddard, T. D., Huang, C. C., Couch, G. S., Greenblatt, D. M., Meng, E. C., and Ferrin, T. E. (2004) *J. Comput. Chem.* **25,** 1605–1612
30. Fushman, D. (2003) in *BioNMR in Drug Research* (Zerbe, O., ed) Wiley-VCH, Weinheim, Germany
31. Lipari, G., and Szabo, A. (1982) *J. Am. Chem. Soc.* **104,** 4546–4559
32. Barbato, G., Ikura, M., Kay, L. E., Pastor, R. W., and Bax, A. (1992) *Biochemistry* **31,** 5269–5278
33. Stone, M. J., Fairbrother, W. J., Palmer, A. G., 3rd, Reizer, J., Saier, M. H., Jr., and Wright, P. E. (1992) *Biochemistry* **31,** 4394–4406
34. Ayed, A., Mulder, F. A., Yi, G. S., Lu, Y., Kay, L. E., and Arrowsmith, C. H. (2001) *Nat. Struct. Biol.* **8,** 756–760
35. Sharma, D., and Rajarathnam, K. (2000) *J. Biomol. NMR* **18,** 165–171
36. Sekerina, E., Rahfeld, J. U., Müller, J., Fanghänel, J., Rascher, C., Fischer, G., and Bayer, P. (2000) *J. Mol. Biol.* **301,** 1003–1017
37. Kühlewein, A., Voll, G., Hernandez, Alvarez, B., Kessler, H., Fischer, G., Rahfeld, J. U., and Gemmecker, G. (2004) *Protein Sci.* **13,** 2378–2387
38. Kazimierczuk, K., Zawadzka, A., Koźmiński, W., and Zhukov, I. (2008) *J. Am. Chem. Soc.* **130,** 5404–5405
39. Ding, K., and Gronenborn, A. M. (2004) *J. Am. Chem. Soc.* **126,** 6232–6233
40. Koźmiński, W., Zhukov, I., Pecul, M., and Sadlej, J. (2005) *J. Biomol. NMR* **31,** 87–95
41. Shen, Y., and Bax, A. (2010) *J. Biomol. NMR* **46,** 199–204
42. Tossavainen, H., Permi, P., Purhonen, S. L., Sarvas, M., Kilpeläinen, I., and Seppala, R. (2006) *FEBS Lett.* **580,** 1822–1826
43. Heikkinen, O., Seppala, R., Tossavainen, H., Heikkinen, S., Koskela, H., Permi, P., and Kilpeläinen, I. (2009) *BMC. Struct. Biol.* **9,** 17
44. Buck, M., Boyd, J., Redfield, C., MacKenzie, D. A., Jeenes, D. J., Archer, D. B., and Dobson, C. M. (1995) *Biochemistry* **34,** 4041–4055
45. Wong, K. B., Fersht, A. R., and Freund, S. M. (1997) *J. Mol. Biol.* **268,** 494–511
46. Ghalebani, L., Kotsyubynskyy, D., and Kowalewski, J. (2008) *J. Magn Reson.* **195,** 1–8
47. Kneller, J. M., Lu, M., and Bracken, C. (2002) *J. Am. Chem. Soc.* **124,** 1852–1853
48. Ranganathan, R., Lu, K. P., Hunter, T., and Noel, J. P. (1997) *Cell* **89,** 875–886
49. Siddiqui, K. S., and Cavicchioli, R. (2006) *Annu. Rev. Biochem.* **75,** 403–433
50. Holm, L., and Park, J. (2000) *Bioinformatics.* **16,** 566–567
51. Yongye, A. B., Bender, A., and Martinez-Mayorga, K. (2010) *J. Comput. Aided Mol. Des.* **24,** 675–686